*Research Article*

Journal of Chemistry Letters
journal homepage: www.jchemlett.com
ISSN (online) 2717-1892 (print) 2821-0123

# Synthesized iron oxide nanoparticles from *Acacia nilotica* leaves for the sequestration of some heavy metal ions in aqueous solutions.

Paul Ocheje Ameh[1,*]

[1] *Physical Chemistry Unit, Department of Chemistry, Nigeria Police Academy, Wudil, P. M B. 3474, Kano State Nigeria*

ARTICLE INFO

*Article history:*
Received 10 November 2022
Received in revised form 25 December 2022
Accepted 30 December 2022
Available online 2 April 2023

*Keywords:*
*Acacia nilotica*
Heavy metal
Adsorption
*nanoparticles,*
*low-cost adsorbents*

ABSTRACT

A batch adsorption system was applied to study the adsorption of Cd (II) , Co(II) and Pb(II) ions from aqueous solutions by iron oxide nano particle (IONP) synthesized from Acacia nilotica plant leaves. The influence of various operating parameters such as contact time, temperature, pH, adsorbent dosage and initial concentration of metal ions and on the adsorption capacity of IONP was investigated. The synthesized adsorbent was characterized by Energy Dispersive X-ray spectroscopy (EDX), Scanning Electron Microscopy (SEM), Fourier Transform Infrared (FT-IR) and X-Ray Diffraction (XRD). Results obtained clearly show that IONP is an effective adsorbent for the removal of the studied metal ions from aqueous solutions. The ease of adsorption of the studied metals onto IONP was found to be in this order: Co (II) > Cd (II) > Pb (II). The kinetic data corresponded well with the pseudo-second order equation, suggesting that the adsorption process is presumably achemisorption. The values oobtained from the thermodynamic parameters ($\Delta G^0_{ads}$, $\Delta S^0_{ads}$, and $\Delta H^0_{ads}$) established that the adsorption process is feasible and endothermic in nature. The adsorption equilibrium data best fitted Freundlich adsorption isotherm. IONP may be a cost-effective alternative for waste water treatment.

## Introduction

The current pattern of industrial activities has alters the natural flow of materials and introduces novel chemicals into the environment leading to pollution of the environment [1]. Pollutants (including heavy metals) in the environment are of major concern because of their toxicity, bio-accumulating tendency and threat to human and animal life [2]. Their presence has led to decrease the supply of useable water, increase the cost of purifying it, contaminate aquatic resources and affect food supplies [3]. Different techniques, including adsorption [4], ion exchange [3], membrane processes [5], chemical precipitation [6], photocatalytic degradation [7], reverse osmosis [8], coagulation [8], solvent extraction [9], flotation [10] and advanced oxidation [11,12], have been applied for adsorbing heavy metal ions from aqueous media. Among these methods, adsorption has been considered as the most efficient method for the removal of contaminants from water. Different forms of biomass have been used for the removal of heavy metals from waste water, although there have been concerns of their low performance in terms of lower surface area to its volume ratio which is been overcome by the use of nano technology techniques [13]. Recently, there is increasing attention of the use of metal and metal oxides nano particles in heavy metal removal from aqueous solutions due to their high performance and low cost for contaminant removal [14].

The aim of this work is to investigate the possibility of using iron oxide nano particle synthesized for the first time from Acacia nilotica plant leaves for the removal lead (II), Cadmium (II) and chromium (II), from aqueous solution. Acacia nilotica is found in various parts of Nigeria spanning from the rainforest through the savnannah up to the arid vegetation zones [15]. The leaves of this plant are not edible and constitute disposal problems as they are found to litter the premises of where ever they are found in the country. One advantage of this adsorption technique being proposed n this research is the use of waste to clean up another waste hence resulting to environmental sustainability. The structure and composition of the synthesized iron oxide nano particle

*Corresponding author. E-mail: amehpaul99@gmail.com
10.22034/jchemlett.2023.360137.1083

(IONP) were characterized by X-Ray Diffraction (XRD), Scanning Electron Microscopy (SEM) and Fourier Transform Infrared (FTIR). The adsorption mechanism of IONP for the heavy metals was discussed through the adsorption kinetic equation, the adsorption isothermal equation, and the [l]thermodynamic equations of adsorption process. It is expected that the synthesized adsorbent will imparts size-dependent properties such as higher adsorption tendency and large volume wastewater treatment systems.

## 2.0 MATERIALS AND METHODS

### 2.1 Preparation of *Acacia nilotica* aqueous Leaf Extract

The leaves of *Acacia nilotica* plant were obtained from the premises of Nigeria Police Academy Wudil Kano State Nigeria. After identification at the Herbarium of Department of Biological Science, they were washed, dried in a laboratory oven at 70 $^{o}$C for 2 days and thereafter grounded into fine particles. The fine powder were further dissolved in a in a 500 mL flat bottom flask using deionized water, heated and stirred in a water bath at 80 $^{o}$C for 1 hour. The aqueous leaf extract was filtered using filter paper, put into an amber bottle, and stored in the refrigerator until further use.

### 2.2. Synthesis of iron oxide nanoparticles.

The method employed in the synthesis of the iron oxide nanoparticle is as described by Guo and Barnard [16]. 100 ml of 0.01 M of $FeCl_3.6H_2O$ was poured into a bottom flask and heated with a mechanical stirrer at 70 $^{o}$C. 40 mL of the *Acacia nilotica* aqueous leaf extract was added in drops to the stirring iron solution and thereafter the mixture was basify to pH of 11 using few drops of 0.1 M NaOH. The mixture was stirred for 1 hour and the resulting product was isolated with the centrifuge, severally washed with deionized water to remove any unreacted salt and metabolites, and. The obtained black powder was dried in the oven at 80 $^{o}$C for 1 day and subjected for further characterization.

### 2.3 Characterization of the synthesized iron oxide nano particle

#### 2.3.1 Scanning Electron Microscope (SEM) - Energy Dispersive X-ray Analysis

The surface texture, elemental content and porosity of the synthesized nano particle was analyzed with the aid of a Phenom Pro X Scanning Electronic Microscope that is fully integrated with Energy Dispersive X-ray (EDX). A thin layer of platinum was sputter-coated on the samples for charge dissipation during SEM imaging. The Energy dispersive Spectrum was obtained alongside with the Element Identification Spectrum.

#### 2.3.2 Fourier transform infra-red (FTIR) analysis

FTIR analyses to elucidate the functional group of the adsorbent was carried out using Scimadzu FTIR- 8400S Fourier transform infra-red spectrophotometer. The sample was prepared using KBr and the analysis was done by scanning the sample through a wave number range of 400 – 4000 $cm^{-1}$.

#### 2.3.3 X-ray diffraction (XRD) study

The structure and identify the phase purity of the synthesized iron nanoparticle was analyzed using a PAN analytical X'pert PRO diffractometer in Bragg- Brentono geometry with a Cu $K_\alpha$ radiation wavelength $\lambda_{\alpha1}$ = 1.5405 Å, $\lambda_{\alpha2}$ = 1.5443 Å. . The samples were placed on a flat plate while intensity data were collected as a function of the Bragg angle, θ, in the range 2θ = 10° to 70° with a step size of 0.013°. The structures obtained were refined with the full-profile Rietveld method using the general structure analysis system with the EXPGUI interface [17]. The crystallite size (D) of the synthesized iron oxide nanoparticles was determined using the Scherrer's equation stated below

$$D = \frac{0.9 \times \lambda}{\Delta \cos \theta} \quad 1$$

Where Δ is the full width at half maximum, λ is the X-ray wavelength, and θ is the Bragg's angle

### 2.4 Batch experiments

The batch test was carried out to determine the adsorption capacity of Co (II), Pb (II) and Cd (II) onto IONP using the method as described by Oladunni *et al* [18]. The effects of batch parameters were investigated by changing adsorbent dosage (0.2 – 1.5 g), contact time (10 – 120 mins), pH (2–9), initial metal ions concentration (10 - 100 mg/L) and temperature (303 – 353 K). In each experiment, weighed quantity of adsorbent was added to a specific volume of working solution and after adjusting the desired pH, the mixture was agitated for specific time. The solution thus obtained was filtered through Whatman filter paper No. 41. Residual concentrations of the analyte ions were measured by using Atomic Absorption Spectrometer, (Model: Analyst 100 PerkinElmer).

The amount of the metal ions absorbed ($q_e$) in milligram per gram of the adsorbent and the percentage of metal ions removed (% Rem) were calculated using equation 2 and 3 respectively [19]:

$$q_e = \frac{V(C_0 - C_e)}{1000} \quad 2$$

$$\%\, Rem = \frac{V(C_0 - C_e)\ x\ 100}{C_0} \quad 3$$

where $C_0$ and $C_e$ (mg/L) are the liquid – phase concentrations of metal ions at initial and any time *t*, respectively; *V* the volume of the solution (L).

## 3.0 RESULTS AND DISCUSSION

### 3.1 Characterization of IONP nanoparticle

The crystal structure of the synthesized IONP was determined using an X-ray diffraction (XRD) technique and the result obtained is as presented in Figure 1. The XRD patterns obtained in the study are similar with that reported in the literature for iron oxide nanoparticle (Dinali et al 2017). The peaks obtained were identified by comparing them with the Joint Committee on Powder Diffraction Standards (JCPDS) files [20]. Six distinct peaks at 2θ = 30°, 36°, 43°,54°, 57° and 63° with the phase plane of (220), (311), (400), (422), (511) and (440) respectively were obtained. None of the peaks corresponding to impurities were found; showing that high-quality was generated. The average particle size of iron oxide nanoparticles as calculated from equation 1 was found to be 11 nm which confirmed that the synthesized nanoparticles were nano crystalline in nature.

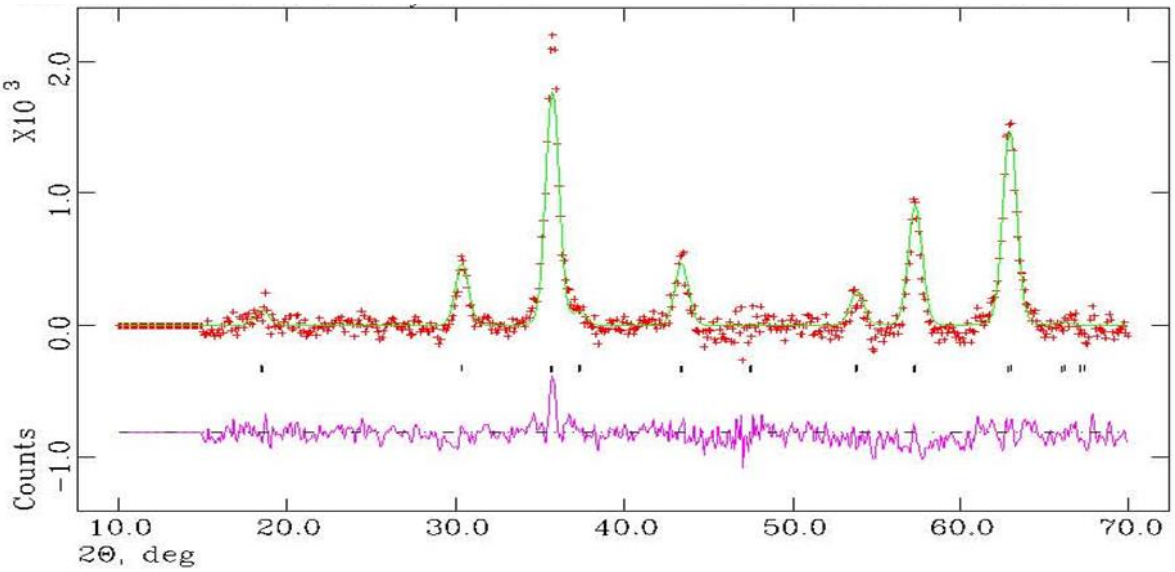


Figure 1: Rietveld refinements of the synthesized iron oxide nano particle against XRD data.

The result obtained from the study of the morphology and texture of both the dry plant extract and the synthesized iron oxide nanoparticle (IONP) using SEM is as presented in Figures 2a and 2b respectively. It can be seen that the SEM images obtained are well dispersed and predominantly spherical in shape. The images for the synthesized size particles (Figure 2 a) were of lesser size compared to the one for the dry raw plant extract (Figure 2b) which is an indication that the IONP will be a better adsorbent as it is likely to have increased surface.porosity[21]

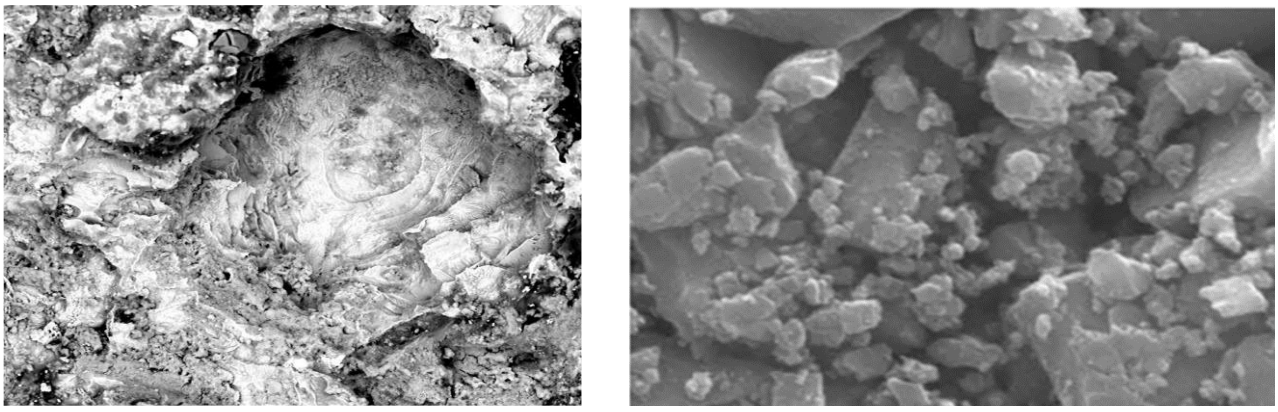

Figure 2: SEM images of (a) synthesized iron oxide nanoparticle (b) dry plant extract

From the result obtained from the EDS analysis of IONP (Figure 3), it can be deduced that IONP consist of iron

as the major metallic element with a percentage of 46.80 %. There is also 36.47 % of oxide and the remaining percentage belonging to Carbon and Sulphur

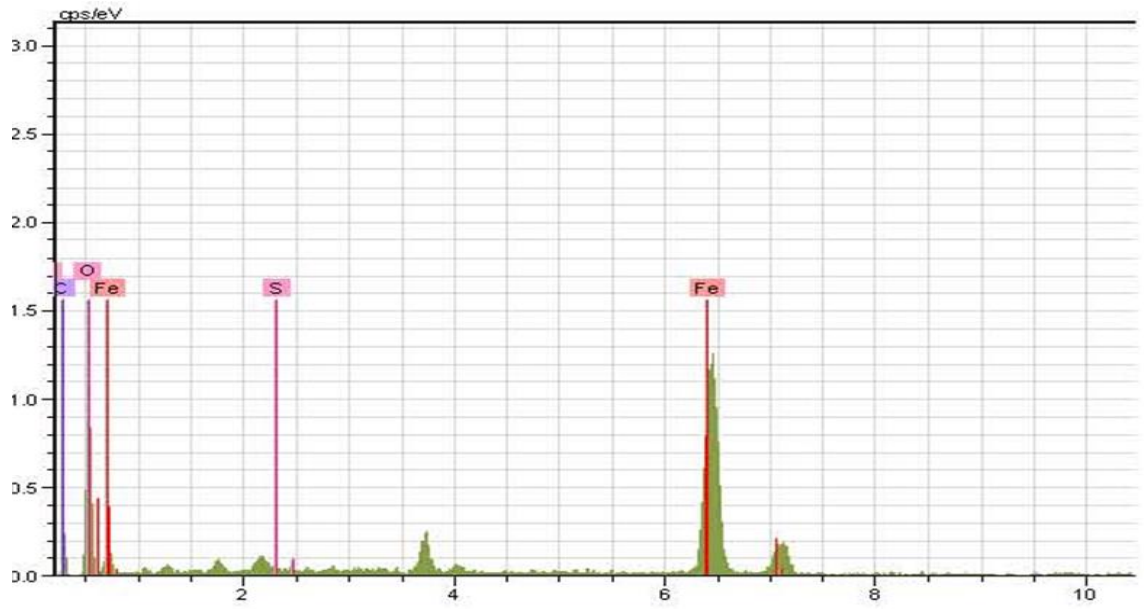


Figure 3 : EDX image of synthesized iron oxide nanoparticle

The FTIR spectrum of the dry plant extract and the synthesized nanoparticle (IONP) is as shown in Figures 4 a and b. The difference between the spectra could be considered as proof of the transformation of the plant extract to nano particle. Frequencies of adsorption deduced from the spectrum as well as bonds / functional group assignments are presented in Table 1. The presented results shows several stretches and vibrations, some of which include C – C bending, $CO_2$ bending =CH out of plane, C-O stretch, C-H wag, C-H in plane bending ($CH_3$) C=C stretch, C-H aliphatic stretch and O-H stretch. The absorption peak at 1635.95 $cm^{-1}$ for instance observed in the spectrum of the raw plant extract can be assigned to amide C=O stretching indicating the presence of –COOH group in the leaf extract. The decreasing intensity of this peak to 1631.83 $cm^{-1}$ in the spectrum of the synthesized nanoparticle signifies the involvement of amide C=O stretching in the reduction process. The observed occurrence of a strong peak at 602.77$cm^{-1}$ denote to the Fe – O stretching band of iron oxide nanoparticles [16].

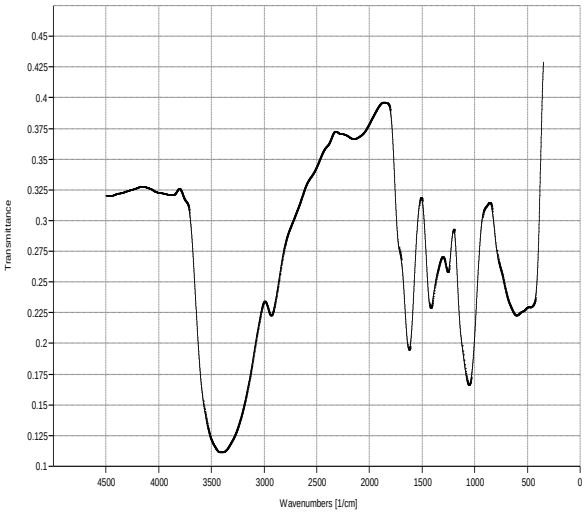


(a)

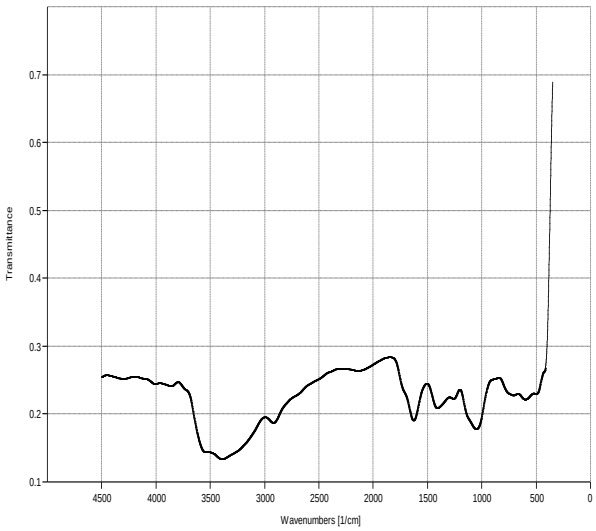


Figure 4: FTIR spectrum of (a) synthesized iron oxide nanoparticle (b) crude plant extract

Table 1: Peaks and functional group assignment of IR adsorption by the synthesized iron oxide nanoparticle and crude plant extract

| Frequency ($cm^{-1}$) | | Functional group assignment |
|---|---|---|
| **Plant extract** | **IONP** | |
| 424.35 | | C-C bending |
| 565.16 | | $CO_2$ bending |
| | 602.77 | Fe – O stretch |
| 887.28 | 715.61 | =CH out of plane |
| 1054.13 | 1054.13 | C-O stretch |
| 1285.6 | 1268.24 | C-H wag |
| 1401.33 | | C-H in plane bending (CH3) |
| 1635.69 | 1631.83 | C=O stretch |
| 2920.32 | 2923.22 | C-H aliphatic stretch |
| 3391.94 | 3394.83 | O-H stretch |
| 3870.3 | | Asymmetric O-H stretching |

### 3.2 Batch equilibrium studies

#### 3.2.1 Effect of initial pH

The effect of initial pH on the adsorption capacity of the studied adsorbent were investigated for Pb (II), Co (II) and Cd (II) ions solutions within a the pH range of 2 – 9. The amount of heavy metal adsorbed was plotted against pH and presented in Figure 5. From the Figure, it could be seen that the amount of the metal ions adsorbed increased along with the increase of pH of the adsorbate solution up to certain value and thereafter start to decrease. This pH dependency observed could be explained as follows. Hydrogen ions occupy most of the adsorption sites on the surface of the adsorbent at low pH values. This makes the metal ions which are positively charged less adsorbed because of electric repulsion with protons on the adsorbent surface. As the pH values of the media is increased, the surface of the adsorbent becomes more negatively charged, hence making the adsorption of the metal ions to increase reaching equilibrium at pH 6.0, 5.0 and 6.0 for cadmium, lead and cobalt respectively. The decrease in adsorption of the metal ions at higher pH has been reported by several researchers to be due to the formation of soluble hydroxylated complexes of the ions and their competition with the active sites [22 – 24]. This will reduce the retention of the metal ions on the surface of the adsorbent. The trend for the adsorption of the metal ions with pH followed the order Co(II) > Cd(II) > Pb (II).

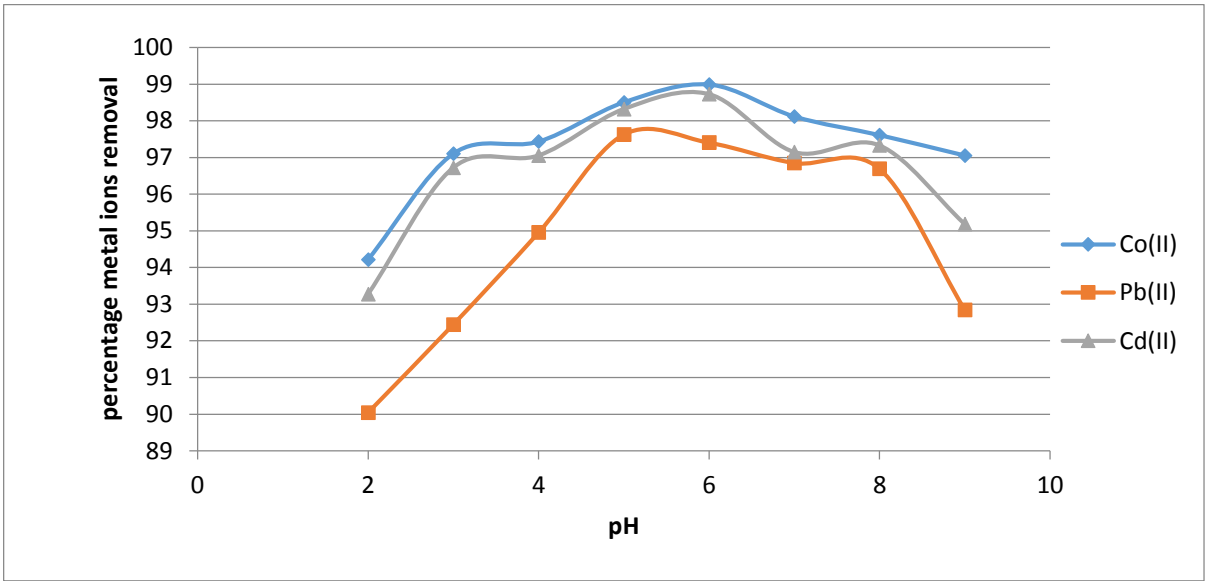


Figure 5: Plot of % adsorption of metal ions versus pH onto IONP

### 3.2.2 Effect of adsorbent dosage

The plots obtained from the investigation of the effects of adsorbent dosage (0.2 g to 1.5 g) on the adsorption of the studied metal ions by the synthesized nanoparticle at constant initial metal ion concentration, solution pH, and contact time is as presented in Figure 6. It can be observed from the plots that the removal efficiency of the adsorbent increases as the dosage of the prepared nano particle increases up till 0.8 g. The increase in adsorption efficiency is as a result of increase in adsorbent binding sites and sorptive surface area at the adsorbent dose increases [25 – 26]. There was no significant change in the removal of metal ions when the dosage of the adsorbent was increased beyond 0.8 g. This suggests that there exist an optimum dose (0.8 g) after which the maximum adsorption sets in (i.e. the adsorption site becomes saturated). The amount of ions bound to the adsorbent and the amount of free ions remains constant from that point even with further addition of the dose of the prepared nano particle

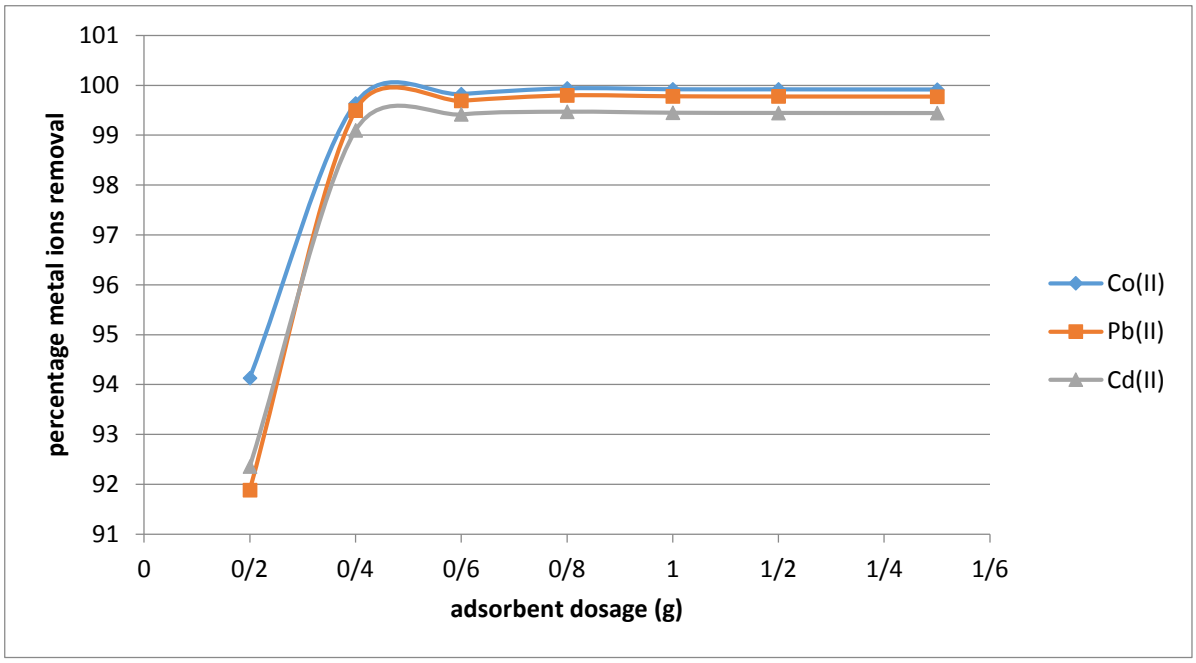


Figure 6: Plot of percentage adsorption of metal ions versus adsorbent dosage onto IONP

### 3.2.3 Effect of temperature

Figure 7 shows the variation of the concentrations of $Cd^{2+}$, $Co^{2+}$ and $Pb^{2+}$ adsorbed by the studied adsorbent from aqueous solutions at various temperatures. It is

evident from the result presented that increase in temperature leads in increase in the amount of heavy metal (adsorbate) uptake which is an indication that the adsorption process is endothermic. This observed increase of amount of metal ions removed with increase in temperature may be due to the increase in kinetic energy of adsorbate ions. This leads to an increase in the frequency of collision between adsorbate and adsorbent resulting in improved adsorption of the metal ions on the adsorbent surface [18].

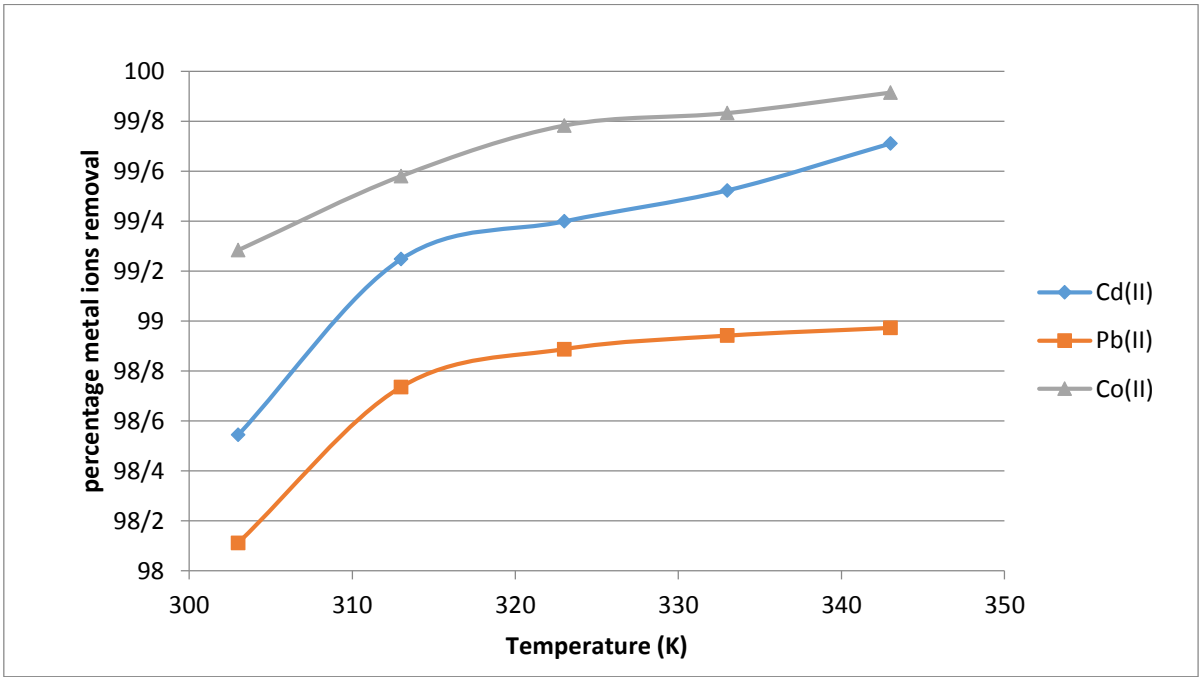


Figure 7: Variation of the amount of heavy metal ion adsorbed per unit mass of the adsorbate (IONP) with temperature

### 3.2.4 Effect of initial metal ion concentration

The influence of adsorbate initial concentration on the adsorption of Co (II), Pb(II) and Cd (II) ions onto the prepared nano particle is illustrated in Figure 8. The adsorption of the heavy metals ions onto the adsorbent was carried out at different concentrations of the metal ions varying from 20 to 100 mg /L at pH 6. Results (Figure 8) showed that the initial metal ions concentration remarkably influenced the equilibrium metal uptake and adsorption yield as the amount of metal ion adsorbed was found to increase with increase in initial concentration. This observation may be due to higher interaction between the metal ions and adsorbent [27]. Similar phenomenon have been reported for was observed for chitosan / raphia palm composite, rice husk, sawdust and egg shell nano particle [3, 4, 21] . The percentage of metal ions removed has been found to higher than those reported by some adsorbent in literature [3].

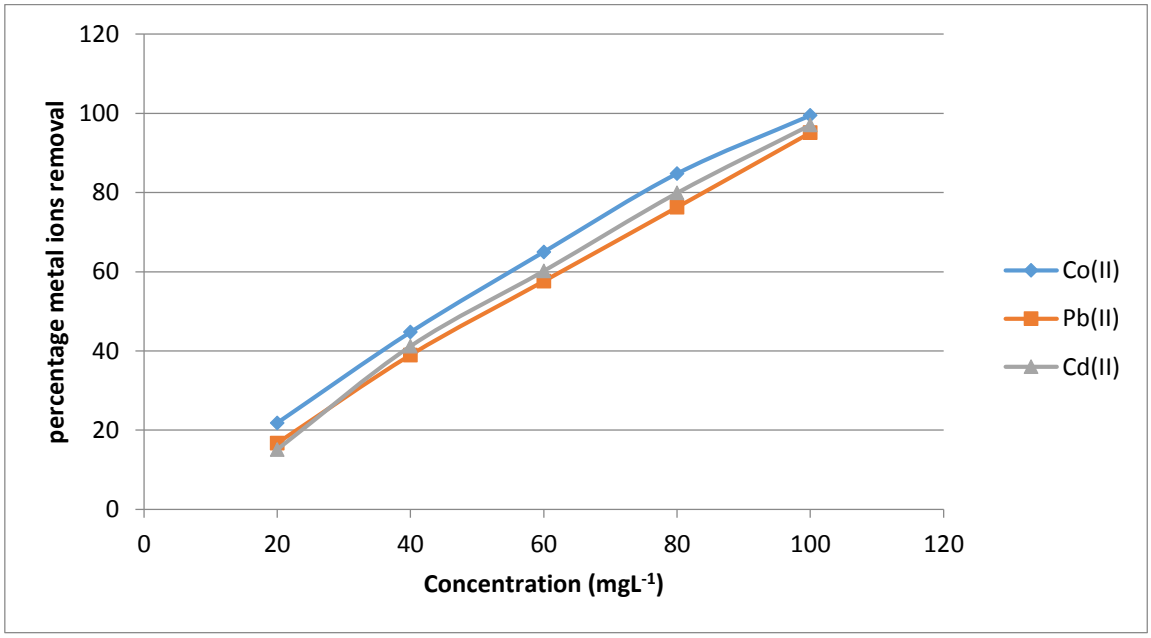


Figure 8: Variation of amount of heavy metal ion adsorbed (by IONP) with concentration of the metal ion in solution

### 3.2.5 Effect of contact time

The test on the effect of the contact time is significant in adsorption studies as it reveal the equilibrium time of the adsorbent which is one of the important parameters for an economical wastewater treatment system. The effects of contact time on the amount of metal ions on adsorbent surface are shown Figure 9. It can be seen that the amount of metal ions adsorbed by the adsorbent maintained a regular increase with increase in contact time before equilibrium is reached. Optimum contact time was found to be 90 minutes a value lower than those reported by many researchers [4]. This means that the synthesized nano particle has a higher surface area to its volume ratio which has significantly improved its binding capacity and the adsorption process proceeded rapidly.

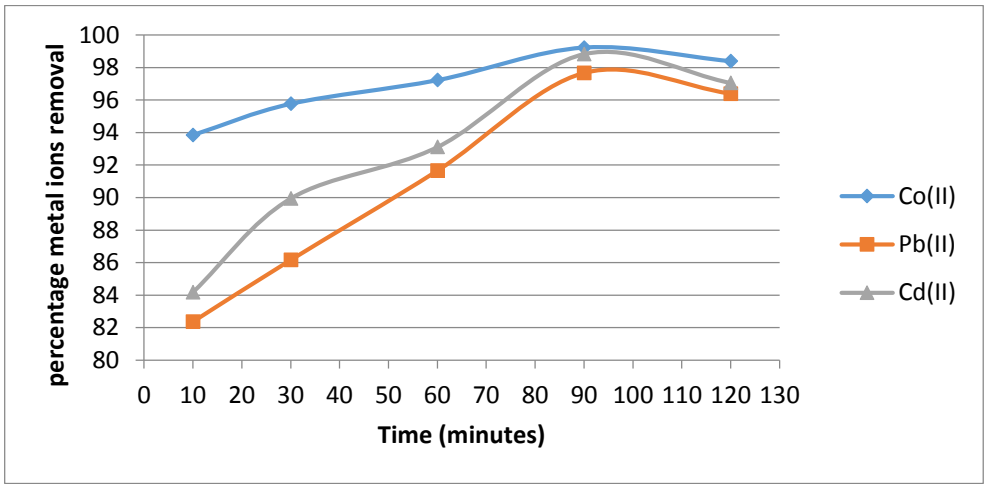


Figure 9: Variation of the amount of heavy metal ion adsorbed per unit mass of the adsorbent (IONP) with time

### 3.3 Adsorption Kinetics

In order to analyze the mechanism of metal ions adsorption onto IONP, and to predict the rate at which the solute ($Pb^{2+}$, $Co^{2+}$ and $Cd^{2+}$) were removed from aqueous solution, the adsorption data were tested with three kinetic models viz: pseudo-first-order kinetic model [28] and pseudo-second-order kinetic model [29] whose linearized forms are given in equation 6 and 7 respectively.

$$\log(q_e - q_t) = \log(q_e) - \left(\frac{k_1}{2.303}\right)t \quad (6)$$

$$\frac{t}{q_e} = \left(\frac{1}{k_2 q_e^2}\right) + \left(\frac{1}{q_e}\right)t \quad (7)$$

where $q_e$ and $q_t$ are the amount of heavy metal ions adsorbed at equilibrium and at time, t respectively in mg/g, $k_1$ is the first order rate constant ($min^{-1}$), $k_2$ is the second order rate constant, C is the boundary layer constant(mg/g), t is the time (min).

The implication of equation 6 is that a plot of $\log(q_e - q_t)$ versus t should be a straight line with slope and intercept equal to $k_1/2.303$ and $\log(q_e)$ respectively. From equation 7, a plot of $\frac{t}{q_e}$ versus t is expected to be linear with slope and intercept equal to $\frac{1}{q_e}$ $and$ $\frac{1}{k_2 q_e^2}$ respectively.

The pseudo-fist-order and pseudo-second-order plots obtained for the adsorption of the studied heavy metals onto IONP are presented in Figure 10 and 11 respectively. Values of rate constants, amount of heavy metal ions adsorbed and correlation coefficients ($R^2$) deduced from the plots is as presented in Table 2. In comparing the results of pseudo-first-order with the pseudo- second-order, it can be observed that the adsorption of Pb (II), Cd (II) and Co (II) fitted better to the pseudo-second-order kinetic model as it showed excellent linearity with higher correlation coefficient ($R^2$) values. The applicability of the pseudo-second-order model suggests that the studied metals attached onto IONP surface by chemical bond [2]. This implies that the heavy metal ions attached to the solid( adsorbent) surface by forming covalent bonds and have tendencies to find sites which maximize their coordination number with the surface ( Wong, 2003). It has been reported that the lower the amount of heavy metal ions adsorbed at equilibrium ($q_e$), the greater the adsorption [29]. This implies that the ease of adsorption of the studied metals onto IONP will be: Co (II) > Cd (II) > Pb (II) . This is because Co (II) ions were discovered to have the least $q_e$ values and Pb (II) the highest $q_e$ values.

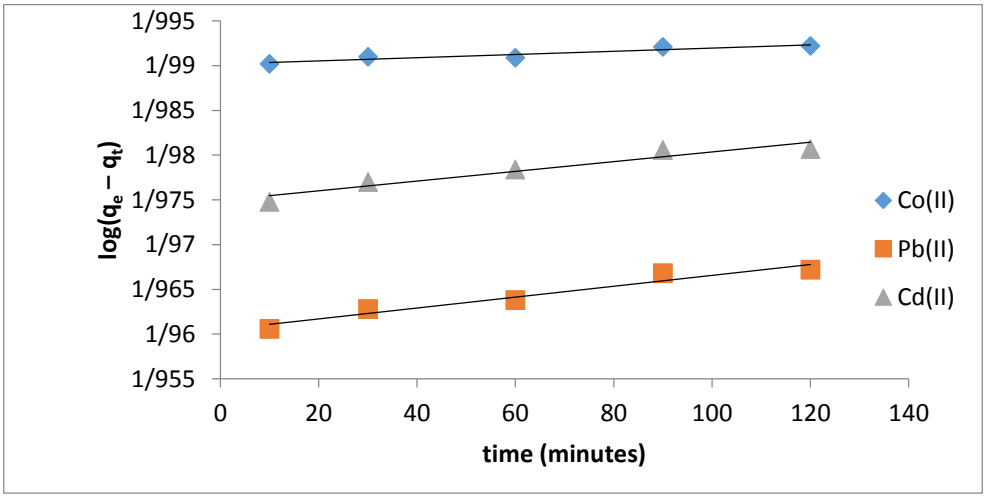


Figure 10: Pseudo first plots for the adsorption of the studied heavy metal ions by IONP

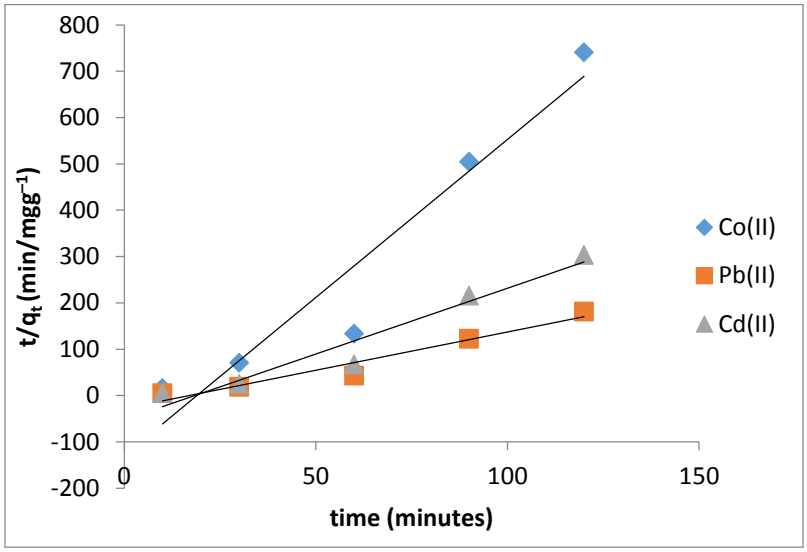


Figure 11: Pseudo second order plots for the adsorption of the studied heavy metal ions by IONP

Table 2: Pseudo first and second order parameters for the adsorption of some heavy metal ions by *iron oxide nanoparticles (IONP)*

| | **Pseudo first order** | | | **Pseudo first order** | | | | | |
|---|---|---|---|---|---|---|---|---|---|
| Cation | $q_e$ (mg/g) | $k_1$ ($min^{-1}$) | $R^2$ | $q_e$ (mg/g) | $k_2$ ($gmg^{-1}min^{-1}$) | $R^2$ | $C_o$(mg/g) | k ($gmg^{-1}min^{-1/2}$ ) | $R^2$ |
| Co(II) | 84.52 | 2.313 x $10^{-4}$ | 0.9024 | 90.98 | 4.615 x $10^{-4}$ | 0.9232 | 0.793 | -0.058 | 0.8807 |
| Cd(II) | 92.67 | 1.304 x $10^{-4}$ | 0.9255 | 94.27 | 1.402 x $10^{-4}$ | 0.9480 | 2.190 | -0.173 | 0.9734 |
| Pb(II) | 96.84 | 1.214 x $10^{-4}$ | 0.9467 | 98.28 | 1.224 x $10^{-4}$ | 0.9423 | 2.661 | -0.186 | 0.9578 |

### 3.4 Thermodynamic consideration

To further account for the effect of temperature on the equilibrium adsorption of $Cd^{2+}$, $Co^{2+}$ and $Pb^{2+}$ onto IONP, the thermodynamic equilibrium constants such as

the standard enthalpy ($\Delta H^0_{ads}$) and entropy ($\Delta S^0_{ads}$) changes were estimated using the transition state equation given by equation 4 [4]

$$log\frac{k}{T} = log\frac{R}{Nh} + \frac{\Delta S^0_{ads}}{2.303R} - \frac{\Delta H^0_{ads}}{2.303RT} \quad 4$$

where k is the adsorption rate constant, T is the temperature, R is the gas constant, N is the Avogadro's number, h is the plank constant. The $\Delta H^0_{ads}$ and $\Delta S^0_{ads}$ values were obtained from the slope and intercept from the transition state plot (Figure 12) and are presented in

Table 3. The standard free energy change of spontaneity values ($\Delta G^o$) for the adsorption process were calculated using the equation 5 and the values obtained are also presented in Table 3

$\Delta G^0 = RT Ink$ 5

From the results obtained, it can be seen that the enthalpy of adsorption ($\Delta H^0$) were positive which further confirm the endothermic nature of the adsorption process. The positive values of $\Delta S^0$ showed the high affinity of the metal ion for the adsorbents used and increase randomness at the solid/ liquid interface during the sorption process [30]. The negative value of $\Delta G^0$ indicates the spontaneous nature of the adsorption process.

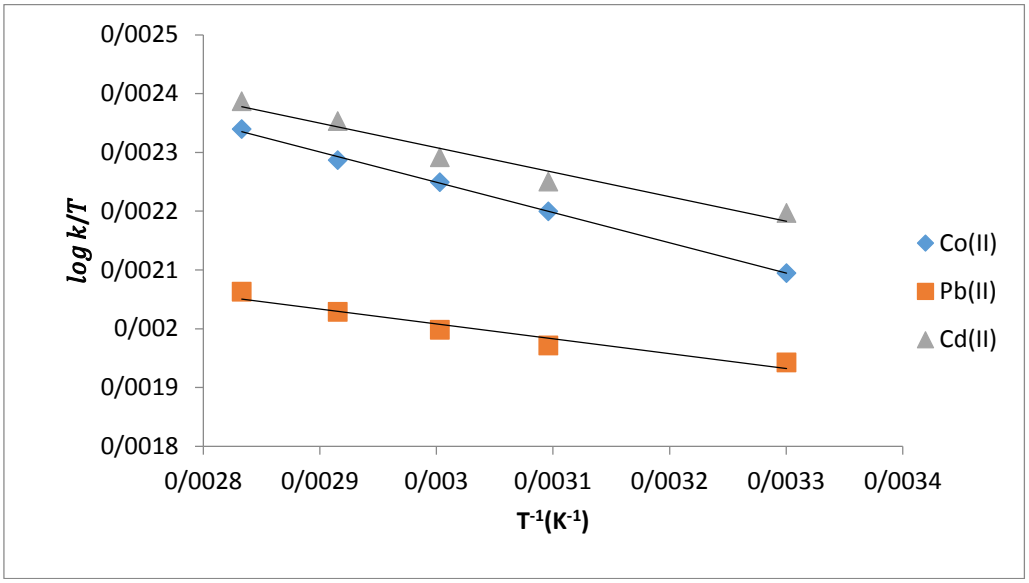


Figure 12: Variation of log(K/T) with 1/T for the absorption of Pb, Ni and Cd ions by IONP

Table 3 : Transition state parameters for the adsorption of Cd, Pb and Co ions by IONP

| Ions | $\Delta H^0$ (kJ/mol) | $\Delta S^0$ (J/mol) | $R^2$ | $\Delta G^0$ (kJ/mol) | | | | |
|---|---|---|---|---|---|---|---|---|
| | | | | 303 K | 323 K | 333 K | 343 K | 353 K |
| **Cd (II)** | 7.1822 | 8.2042 | 0.9608 | -1.8335 | -2.0229 | -2.1850 | -2.2696 | -2.3154 |
| **Co(II)** | 6.6096 | 4.5087 | 0.9988 | -1.7231 | -1.7726 | -1.8032 | -1.9101 | -2.1652 |
| **Pb(II)** | 7.1500 | 6.6892 | 0.9428 | -1.7585 | -1.7987 | -1.8215 | -1.9941 | -2.2245 |

### 3.5 Adsorption Isotherm

Experimental data obtained were fitted into Flory–Huggins, Brunauer–Emmett–Teller, Langmuir, Freundlich, Redlich– Peterson, Temkin, Toth, Koble–Corrigan, Sips, Khan, Hill, and Radke–Prausnitz isotherms. From the results obtained, the best isotherm that described the adsorption characteristics of Co (II), Cd (II) and Pb (II) ions onto IONP is Fruendlich adsorption isotherm as a good linear determination coefficient was obtained. The Freundlich isotherm equation is represented by equation 8 (ref)

$$logq_e = logK_F + \frac{1}{n} logC_e \quad 8$$

where $q_e$ is the model ion adsorbed (mg/g), $C_e$ is the equilibrium concentration of metal ion in solution (mg/l), $\frac{1}{n}$ is the heterogeneity factor and $K_F$ is the Freundlich constant (L/g) related to the bonding energy.

The plots of $logq_e$ against $logC_e$ log Ce for the adsorption of Co (II), Cd (II) and Pb (II) ions onto IONP are shown in Figures 13. The values of n and $K_F$ which were calculated from slope and intercept of plots are presented in Table 4. According to Arami et al [31], the values of $\frac{1}{n}$ indicate the type of adsorption process. The process is favorable when $0 < \frac{1}{n} < 1$, unfavorable when $\frac{1}{n} > 1$, and irreversible when $\frac{1}{n} = 0$. The values of $\frac{1}{n}$ which is related to the distribution on bonded ions on the adsorbent surface obtained in the study were found to be less than 1 indicating favourable adsorption. Also the heterogeneity factor values below unity has been reported to be an indication of a chemisorptions process [21].

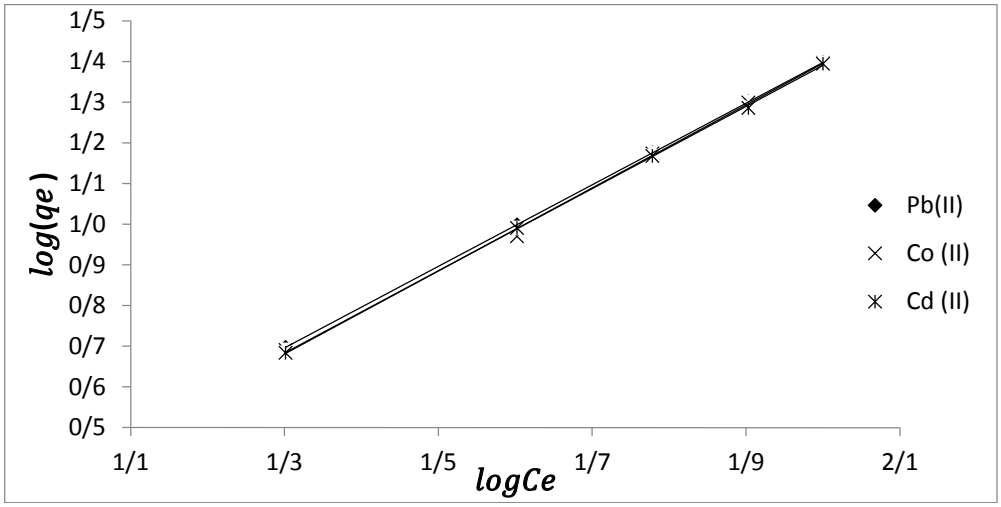


Figure 13: Variation of log($q_e$) with log($C_e$) for the adsorption of the studied heavy metals by IONP

Table 4: Freundlich and Dubinin – Radushkevich (D-R) parameters for the adsorption of the studied heavy metals by IONP

| Metal ion | Freundlich parameters | | | D-R parameters | | |
|---|---|---|---|---|---|---|
| | $\frac{1}{n}$ | Logk | $R^2$ | ln($X_m$) | E (kJ/mol) | $R^2$ |
| **Pb(II)** | 0.9976 | -0.6074 | 1.0000 | 1641.5 | 1.22 | 0.9441 |
| **Co(II)** | 0.9813 | -0.6432 | 0.9995 | 1765.2 | 1.17 | 0.9556 |
| **Cd(II)** | 0.9905 | -0.6293 | 0.9997 | 1638.9 | 1.23 | 0.9358 |

The Dubinin – Radushkevich (D –R) model is used to estimate the characteristics porosity of the biomass and the apparent energy of adsorption, the equation for the model is represented by equation 9 [4].

$$lnq_e = lnX_m - a\left[\mathrm{RTln}\left(1 + \frac{1}{C_e}\right)\right]^2 \quad 9$$

where $q_e$ (mgl/g) is the concentration of the adsorbate adsorbed in the adsorbent, $X_m$ (mg/g) is the maximum adsorption capacity, "a" can be defined as half the square of the reciprocal of the mean adsorption energy

From equation 9, a plot of $lnq_e$ versus ε (where $\varepsilon = \left[\mathrm{RTln}\left(1 + \frac{1}{C_e}\right)\right]^2$) yielding a straight line (see Figure 14) confirms the applicability of the model. The apparent energy (E) of adsorption was computed from the slope using the relationship in equation 11 [4]. The values obtained from these calculations are presented in Table 4

$$a = \frac{1}{2}\left(\frac{1}{E}\right)^2 \quad 10$$

The mean energy adsorption for the uptake of the studied metal ions by IONP as seen in the Table 4 are in the range of 1.17 kJ/mol - 1.23 kJ/mol. These values are within the energy range of chemisorption adsorption reaction. Chemisorption processes have adsorption energies less than 8 kJ/mol while energy values greater than 8 kJ/mol are consistent with the mechanism of physical adsorption Arami et al [31].

The values of $X_m$ (Table 4) which is a measure of the theoretical maximum capacity of adsorbent obtained from the intercept of the Dubinin- Radushkevich plots were high and are within the range of values reported for very good adsorbents [3, 4, 32].

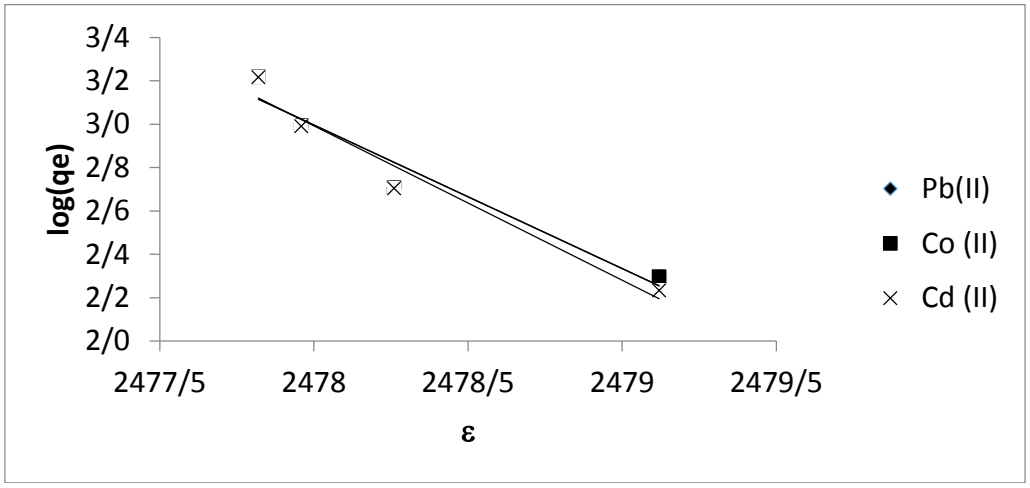


Figure 14: Variation of $\log(q_e)$ with ε for the adsorption of the studied heavy metal ions by IONP

## Conclusion

Synthesized iron oxide nano particle from *Acacia nilotica* leaves have been found to be economically viable and potential adsorbent for the removal of Co(II), Cd(II) and Pb(II) ions from aqueous solutions. The adsorption process has been shown to be affected from experimental conditions, such as pH, initial metal ion concentration, temperature, contact time and adsorbent dose. Thermodynamic studies confirmed that the process was favourable, spontaneous and endothermic. The Freundlich isotherm gave better fits for the adsorption process. The best correlation coefficient was obtained using the pseudo-second order kinetic model indicating that the studied metal ions removal process followed the pseudo-second order rate expression.

## ACKNOWLEDGEMENTS

The research work that generated this publication was fully sponsored by the Tertiary Education Trust Fund of Nigeria (TETFUND) through the Institutional based Research grant

## REFERENCES

1. M. Faisal, S. Hasnain,.Microbial conversion of Cr(VI) into Cr(III) in industrial effluent, *Afri. J Bio*, 3(11) (2004) 610 – 617.
2. J. C. Igwe, D. N. Ogunewed, A. A Abia, Competitive adsorption of Zn (II), Cd (II) and Pb(II) from aqueous and
3. non-aqueous solution by maize cob and husk, *Afri. J Biotechnol* 4 (2005) 1113 – 1116.
4. G. X. Zhao, X. B. Huang, Z.W. Tang, Q. F. Huang, F. L. Niu, X.K. Wang, Polymer-based nanocomposites for heavy metal ions removal from aqueous solution: a review. *Polym. Chem*, 9 (2018) 3562 – 3582.
5. P. O. Ameh. Adsorption of nickel (II), cadmium (II) and lead (II) from aqueous solution using chitosan / raphia palm composite, *Alg. J Mat Chem*, 3(2) (2020) 48–60.
6. M. Montana, A. Camacho, I. Serrano, R. Devesa, L. Matia, I. Vallés, Removal of radionuclides in drinking water by membrane treatment using ultrafiltration, reverse osmosis and electrodialysis reversal. *J. Environ. Radioact*, 125 (2013) 86 – 92.

S. Yu, X. Wang, W. Yao, J. Wang, Y. Ji, Y. Ai, A. Alsaedi, T Hayat, X. Wang, Macroscopic, spectroscopic, and theoretical investigation for the interaction of phenol and naphthol on reduced graphene oxide. Environ. Sci. Technol., 51 (2017) 3278–3286.

7. P. Varjani, S. Suganya, Treatment of dye wastewater using an ultrasonic aided nanoparticle stacked activated carbon:kinetic and isotherm modeling, *Bioresour. Technol*. 250 (2018) 716–722.
8. M. Mohsen-Nia, P. Montazeri, H. Modarress, Removal of $Cu^{2+}$ and $Ni^{2+}$ from wastewater with a chelating agent and reverse osmosis processes. *Desalination*, 217 (2007) 276–281.
9. I. Heidmann, W. Calmano, Removal of Zn(II), Cu(II), Ni(II), Ag(I) and Cr(VI) present in aqueous solutions by aluminium electrocoagulation, *J. Hazard. Mater*. 152 (2008) 934–941.
10. R. Huang, K. Mcphedran, N. Sun, P. Chelmeayala, E Gamal, Investigation of the impact of organic solvent type and solution pH on the extraction efficiency of naphthenic acids from oil sands process erected water, *Chemosphere*, 146 (2016) 472–477.
11. P. S. Sudilovskiy, G.G. Kagramanov, V.A. Kolesnikov, Use of RO and NF for treatment of copper containing wastewaters in combination with flotation. *Desalination*, 221 (2008) 192–201.
12. A. Serrà,. E Gómez, L. Philippe, Bioinspired ZnO-Based solar photocatalysts for the efficient decontamination of persistent organic pollutants and hexavalent chromium in wastewater. *Catalysts*, 9 (2019) 974.
13. M. N. Chong, B. Jin, C.W.K. Chow, C. Saint, Recent developments in photocatalytic water treatment technology: A review. *Water Res*., 44 (2010) 2997–3027.

V. Kamath, P. Chandra, G. P. Jeppu, Comparative study of using five different leaf extracts in the green synthesis of iron oxide nanoparticles for removal of arsenic from water. *Int. J. Phy.* 22 (2020) 1278 – 1294 .

14. P. O Ameh, N. O. Eddy, C. E Gimba. Physiochemical and rheological studies on some natural polymers and their potentials as corrosion inhibitors. Lambert Academic Publishing, UK. 2012

15. H. Guo, A.S Barnard, Naturally occurring iron oxide nanoparticles: morphology, surface chemistry and environmental stability. *J. Mat. Chem. A., 1* (2013) 27-42.
16. B. H. Toby, "EXPGUI , A Graphical User Interface for GSAS," *J. Appl. Crystallogr*. 34 (2) (2001) 210–213,.
17. N. Oladunni, P. O. Ameh, G. Wyasu, J. C Onwuka, Adsorption of cadmium(II) and chromium(VI) ions from aqueous solutions by activated locust bean husk. *Int. J. Modern Chem.*, 3 (2012) 51-64.
18. P .O. Ameh. Modelling of the Adsorption of Cu (II) and Cd (II) from Aqueous Solution by Iraqi Palm-Date Activated Carbon (IPDAC) *Int. J. Modern Chem* 5(3) (2013) 136-144.
19. R. Dinali, A. Ebrahiminezhad, Y. Manley-Harris, Y. Ghasemi, A. Berenjian . Iron oxide nanoparticles in modern microbiology and biotechnology. *Crit. Rev. Microbiol., 43,* (2017) 493-507.
20. R. G. Jalu, A. T. Chamada , R. Kasirajan , Calcium oxide nanoparticles synthesis from hen eggshells for removal of Pb (II) from aqueous solution, *Environ. Challenges* 4 (2021) 1 – 20.
21. T. Mathialagan, T. Viraraghavan, D.R. Cullimore, Adsorption of cadmium from aqueous solutions by edible mushrooms (*Agaricus bisporus* and *Lentinus edodes*), *Water Qual. Res. J. Canada* 38 (2003) 499–514.
22. R. Say, A. Denizli, M.Y. Arica, Biosorption of cadmium (II), lead (II) and copper (II) with the filamentous fungus *Phanerochaete chrysosporium*, *Bioresour. Technol*. 76 (2001) 67–70.
23. S.M. Nomanbhay, K. Palanisamy, Removal of heavy metals from industrial wastewater using chitosan coated oil palm shell charcoal, *Electron. J. Biotechnol*. 8 (2004) 43–53.
24. H. Zhang, L Liu. , L. Jindun, L. Hongping, L. Jie, Equilibrium, kinetics and thermodynamics studies of Lead (II) biosorption on Semame husks. *Bio. Resour*. 7(3) (2012) 3555–3572.
25. P. O Ameh, R. Odoh, A Oluwaseye, Equilibrium Study on the Adsorption of Zn(II) and Pb (II) ions from Aqueous Solution onto *Vitex doniana* Nut *Int. J. Modern Chem* 3(2) (2012) 82-97.
26. S. Tunali, A. C. Abuk, T. Akar, Removal of lead and copper ions from soil, *Chem. Eng. J*. 115 (2006) 203–211
27. R. Labied, O. Benturki, A.Y Eddine, A. Donnot, Adsorption of hexavalent chromium by activated carbon obtained from a waste lignocellulosic material (Ziziphus jujuba cores): Kinetic, equilibrium, and thermodynamic study, *Adsorp Sci Technol*. 36(3-4) (2018) 1066-1099
28. J. C. Igwe, A. A. Abia, Adsorption kinetics and intraparticulate diffusivities for bioremediation of Co (II), Fe (II) and Cu (II) ions from waste water using modified and unmodified maize cob. *Int. J. Phys. Sci.* 2(5) (2007) 119-127.
29. U. Yunusa , U. Bishir, M. B. Ibrahim , Kinetic and thermodynamic studies of malachite green adsorption using activated carbon prepared from desert date seed shell. *Alg J. Eng. Technol*. 2 (2020) 37-45
30. M. Arami, N.Y. Limaee, N.M Mahmoodi, Evaluation of the adsorption kinetics and equilibrium for the potential removal of acid dyes using a biosorbent. *Chem. Eng. J*. 139 (2008) 2–10
31. K Rai, B. S Giri, Y. Nath , H. Bajaj, S. Soni , R.P Singh, R. S Singh, B. N. Rai , Adsorption of hexavalent chromium from aqueous solution by activated carbon prepared from almond shell: kinetics, equilibrium and thermodynamics study. *J. Water Supply: Res Technol.-Aqua*. 67(8) (2018) 724-737.